NANOSYSTEMS: PHYSICS, CHEMISTRY, MATHEMATICS, 2019, 10 (4), P. 466–474

Photoelectrochemical cell performance Cu doped ZnO photoanode sensitized by xanthene dyes

Deepak Kumbhar[1,4], Sarita Kumbhar[2], Sagar Delekar[3], Rekha Nalawade[3], Avinash Nalawade[4]*

[1]Department of Chemistry, Raje Ramrao Mahavidyalaya, Jath, 416 404,
affiliated to Shivaji University Kolhapur 416004, MS, India
[2]Department of Physics, Rajashri Chhatrapati Shahu College, Kolhapur, 416 005,
affiliated to Shivaji University Kolhapur 416004, MS, India
[3]Department of Chemistry, Shivaji University, Kolhapur, 416 004, MS, India
[4]Department of Chemistry, Lal Bahadur Shastri College, Satara, 415 002,
affiliated to Shivaji University Kolhapur 416004, MS, India
*avinashnalawaderes@gmail.com

DOI 10.17586/2220-8054-2019-10-4-466-474

In this study transition metal Cu is doped into ZnO framework at 1, 3 and 5 mol% concentrations by sol-gel method and Photoelectrochemical performance under sensitization is recorded. Structural analysis XRD and Raman gives information of wurtzite structure formation without any mislaid peaks. It also informs decrement in crystalline size and lattice parameters as doping level increases. SEM and EDAX provide nono structure formation with appropriate compositions. Optical analysis by FTIR and PL gives peaks at expected positions while DRS UV-visible peaks show humps with red shift due to effect of Cu doping. After structural and morphological study NPs are deposited on conducting glass surface of FTO substrate by doctor blade method and sensitized with mixed xanthene dyes (Eosine Y., Rhodamine B., and Rose Bengal) for 12 h and photoelectrochemical cell performance are recorded under solar simulator under standard AM 1.5 one sun illumination in that 1 % Cu/ZnO photoanode shows good performance as compared to other.

Keywords: Sol-gel, Cu doped ZnO NPs, xanthene dyes, sensitization, photoelectrochemical cell.

Received: 2 August 2019

Revised: 10 August 2019

1. Introduction

The role of energy is crucial in the human development in all areas of human activity, such as economic, ecosystem, employment, prosperity and equity. For many years, human have utilized several resources to generate energy and fulfil all needs for better life. But, currently, because of increased population the use of traditional resources for energy are not adequate and this creates an issue of global warming [1,2]. Thus, humanity is continuously in the search of alternative energy sources with environmental friendliness. Many research groups already worked on solar, wind, hydro, bio and geothermal energies and catch beneficial outcomes [3–5]. Still this era is under increased pressure to obtain satisfactory outcomes. Solar energy is considered to be more beneficial as compared to other renewable energy sources due to its key benefits of clean, non-polluting, noise less, low maintenance, long life etc. [6, 7]. To acquire this energy role of PV devices are originated. In that solar cell play role to convert solar radiation into electricity. The desire of human fabricated first to fourth generation solar cells with diverse materials and technologies. In the market silicon based solar cells existing but it has limitation to use in wide range due to environmental and cost consequence. O'Regan and Grätzel in 1991 invented low cost and simple construction based dye sensitized solar cell (DSSC). In comparison to silicon cells, it is still in a state of growth to get high efficiency and stability. Researchers are currently working on this and have formulated a number of nanomaterials [8].

In DSSC type of photoanode, electrolyte and sensitizer are crucial to bring beneficial outcome. TiO_2 is typically used photoanode material however it has limitations of carcinogenic nature, lower electron lifetime and transport rate [9–11]. So, research groups worked on several alternative materials. ZnO is another choice with parallel properties of TiO_2 having wide band-gap of 3.37 eV at room temperature, 60 meV of electron binding energy [12, 13], higher electron mobility, anti-oxidation and chemically stability. However, considerable research has revealed lower performance of ZnO based DSSC due to some limitations of ZnO. To circumvent these limitations, different strategies have been developed such as modified fabrication process, utilization of different morphological materials, mixing of other nanomaterial, utilization of new dyes, co-sensitization method, material increased porosity and use of varied electrolyte in DSSC. Doping is one more strategy that offers an effective means to enhance and control the structural, optical and electrical properties of ZnO NPs. Already different dopants (Al, Mn, Cd, Mg, Ni, Ga, Ag, Cr etc.) in the lattice structure of ZnO utilized to boost its properties [14–18]. Doping is one of the methods to modify the band

gap of ZnO and shift to the large visible spectrum of light by creating energy levels inside the band gap [19–21]. Our study focused on doping of Cu due to its large solubility in ZnO matrix, rich electronic states and close ionic radius. Until now, various researchers studied and reported effect of Cu doping on ZnO with respect to morphological and optical properties [22–27]. Assimilation of Cu dopants in ZnO is carried out at low level i.e. 1, 3 and 5 mol% for decrement of band gap and to improve electron shifting. This was successfully carried out by simple sol-gel approach. After structural, morphological and optical analyses, photoanodes were prepared by reported doctor blade technique. To improve DSSC performance and reduce Zn^{2+}-dye aggregation photoanodes were sensitized in metal free sensitization in xanthene dyes and the photoelectrochemical cell performance measured under solar simulator standard AM 1.5 one sun illumination visible illumination of 100 mW/cm^2. Among employed photoanodes 1 % Cu/ZnO shows notable efficiency of $\eta = 0.1165$ % and proves fruitful effect of doping and Co-sensitization.

2. Experimental section

2.1. Materials

All the chemicals i.e. zinc acetate dihydrate (Sigma-Aldrich), copper acetate monohydrate (Sigma-Aldrich), sodium dodecyl sulfate (SDS of SD Fine), ammonium hydroxide (SD Fine) used in the experiment were of analytical grade without any prior treatment.

2.2. Synthesis of Cu doped ZnO NPs by sol-gel method

For this 0.2 M zinc acetate dihydrate (for doping with stoichiometric doping amount of copper acetate monohydrate) solution was prepared and 0.02 M of SDS mixed into it with continuous stirring. To this solution ammonium hydroxide was added drop wise till pH of solution becomes near to 8.0 ± 0.1. Here formation of zinc hydroxide sol takes place, which was further dried at 80 °C for 9 h to get gel. The obtained gel was calcinated at 350 °C for 3 h in a muffle furnace, results in Cu doped ZnO NPs.

3. Results and discussion

3.1. X-ray diffraction analysis

The XRD spectra (Fig. 1) indicate pure and Cu doped (1, 3 and 5 mol%) ZnO NPs. XRD patterns of both undoped and Cu doped samples were found to be exactly same. This data was found to be of hexagonal wurtzite phase and JCPDS card No. 36-1451 [25, 28, 29]. The peak intensities of (100), (002), (101), (102), (110), (103), (200), (112), (201), (004) and (202) in the XRD spectrum are slightly decreased as doping concentration increases this can be also attributed to the replacement of Zn^{+2} by Cu^{+2}. The crystalline size of Cu doped ZnO NPs were obtained by fitting the XRD data to the Debye Scherrer formula and full-width at half-maximum (FWHM) of the XRD lines [30]:

$$D = \frac{0.9\lambda}{\beta \cos\theta}, \tag{1}$$

where λ is the wavelength of X-ray (1.5406 Å), β is the full-width at half-maximum in radian, and θ is the angle of diffraction. It is seen that average crystalline size (D) decreased from 60 to 31 nm as Cu doping. The variation in

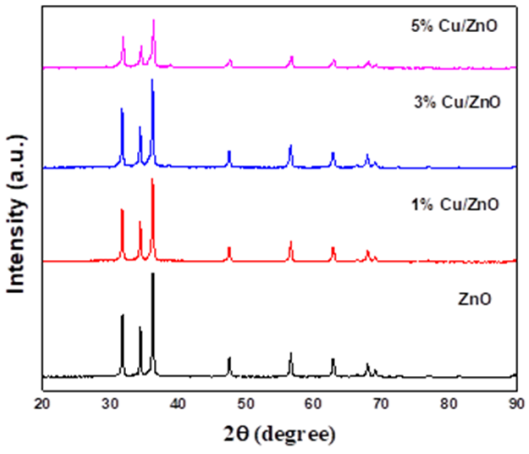

FIG. 1. XRD patterns of pure ZnO and 1, 3, 5 mol% Cu doped ZnO Nanoparticles

the grain size by doping ZnO with Cu^{2+} up to 5 mol% is mainly due to the alteration in the host ZnO lattice, which decreases the nucleation and subsequent growth rate by the addition of Cu concentrations up to 5 mol% as same in some reference [26, 27]. By increasing the Cu content, the carrier concentration and mobility in the conduction band of the semiconductor also increases [31]. The lattice parameters (a, c), volume (V), c/a ratio and crystalline size obtained are given in Table 1. It conclude that values of lattice parameters and volume slightly decreases as doping contartion increases from 1 to 5 mol%. This reduction is due to successful replacement of Zn^{2+} with ionic redii 0.74 Å by Cu^{2+} with ionic redii 0.73 Å [32–35].

TABLE 1. Lattice constant a, c volume of unit cell (V), ratio (c/a) and crystallite size (D) of ZnO and Cu/ZnO sample

Samples	**Lattice Parameter (Å)**		**Volume (Å^3)**	**c/a ratio**	**Crystalline size (D) nm**
	a	***c***			
ZnO	2.9495	5.1065	44.4244	1.732	60
1 % Cu/ZnO	2.9441	5.0993	44.2023	1.732	40
3 % Cu/ZnO	2.9440	5.0961	44.1696	1.732	37
5 % Cu/ZnO	2.9336	5.0811	43.7300	1.732	31

3.2. Raman spectroscopy

Raman spectra in the range of 250 – 600 cm^{-1} of doped and undoped ZnO are showed in Fig. 2. In this range, there are five main bands at 326, 400, 433, 572, 589 cm^{-1}, corresponding to A_1(TO), E_1(TO), E_2(high), E_1(low) and A_1 (low) for ZnO. The strong and sharp band observed at 433 cm^{-1} corresponds to the nonpolar optical phonons E_2 (high) mode of ZnO attribute that incorporation of Cu in ZnO leads to a decrease in crystal quality, but there is no change in wurtzite crystal structure. The features located at 326 and 400 cm^{-1} correspond to the multi-phonon scattering process E_2 (high)–E_2 (low) and A_1 (phonons of ZnO crystal, respectively). The signal located at 572 cm^{-1} could be attributed to the E_1, longitudinal optical phonon (LO) feature, associated with the formation of defects such as oxygen vacancy. According to the literature, as the Cu doping concentration was increased, intensities of spectra decreased and the A_1 transverse optical phonon (TO) mode vanished [36]. It could be successfully explained in terms of resonant anharmonic interaction of the high E_2 mode with a band of combined transverse and longitudinal acoustic modes, as the steep variation of the two-phonon density of states around the high E_2 frequency leads to a distorted phonon line shape [37, 38].

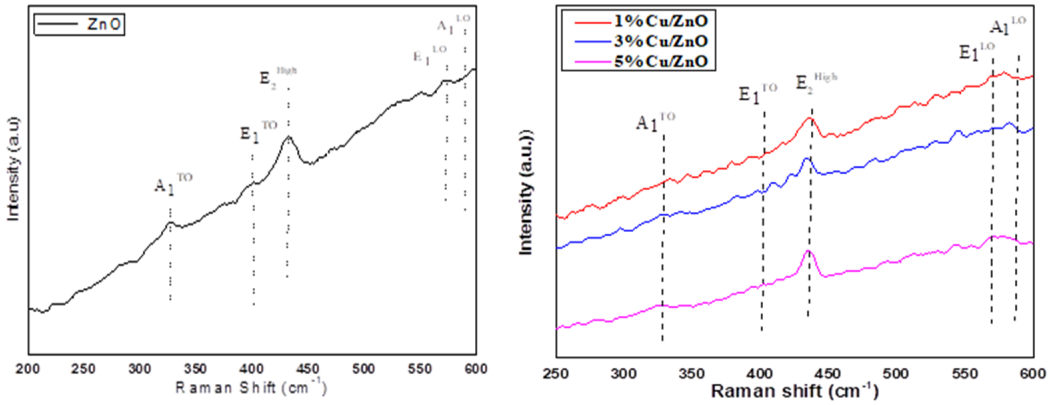

FIG. 2. Raman spectra of the ZnO and Cu doped ZnO NPs

3.3. Scanning electron microscope (SEM) and Energy Dispersive X-Ray Analysis (EDX)

Figure 3 showed that the ZnO and Cu doped ZnO NPs are in regular or almost in granular shape, though some agglomerations have been observed. It was observed that doping of Cu in ZnO slightly affect the size of ZnO NPs, as also suggested by XRD study. It is due to less ionic radii (0.87 Å) of Cu than Zn (0.88 Å) [31]. Fig. 3(b) shows the EDAX spectra of ZnO and Cu doped ZnO nanoparticles. The elements of Zn, O and Cu in doped samples clearly observed. The Compositions are given below (Table 2).

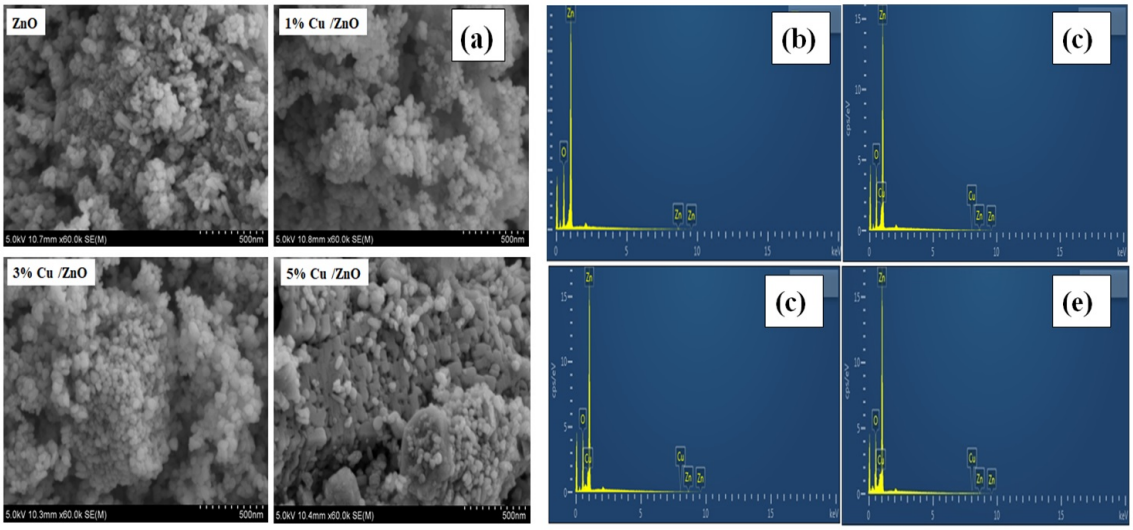

FIG. 3. SEM images of 1, 3 and 5 % Cu/ZnO doped ZnO NPs (a); EDAX images of 1, 3 and 5 % Cu/ZnO doped ZnO NPs (b)

TABLE 2. Composition of ZnO and Cu doped ZnO nanoparticles

Sample	O (Wt %)	Zn (Wt %)	Cu (Wt %)
ZnO	16.84	83.16	—
1 % Cu/ZnO	17.12	82.10	0.87
3 % Cu/ZnO	16.25	81.15	2.60
5 % Cu/ZnO	16.55	79.05	4.40

3.4. Fourier transform infrared spectroscopy (FTIR) studies

The broad absorption peaks in Fig. 4 around 3500 cm^{-1} attributed to normal polymeric O–H stretching vibration of H_2O in Cu–Zn–O lattice and the weak bands from 500 to 881 cm^{-1} are assigned due to the change in the microstructural features Cu doping into Zn–O lattice that shifts frequencies. Copper atom is slightly lighter than Zn atom so, according to the well-established theories of vibrational modes in mixed crystals the substitution should result in an upward shift of the fundamental transverse optical phonon mode. The frequency shift towards the lower side reveals the substitution of Cu^{2+} ion into the Zn–O lattice [39, 40].

3.5. Photoluminescence spectroscopy

ZnO and Cu doped ZnO PL spectra in Fig. 5 displays peaks at ∼300 nm excitation wavelength, in the UV range, which is associated with exciton emission i.e. band edge emission (NBE), another in the visible range at around ∼600 nm, which originates from electron–hole (e–h) recombination at the deep level (DLE) caused by oxygen vacancy or zinc interstitial defect [29, 41]. The lower intensity of UV emission in ZnO than Cu doped ZnO indicated suppression in recombination of photogenerated charge carriers that enhances optical properties [42, 43]. Here 1 % Cu/ZnO samples showed lower recombination rate as compared to other samples.

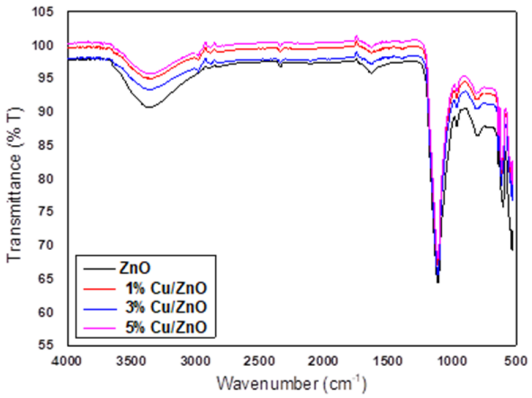

FIG. 4. ATR-FTIR spectra of ZnO and Cu doped ZnO NPs

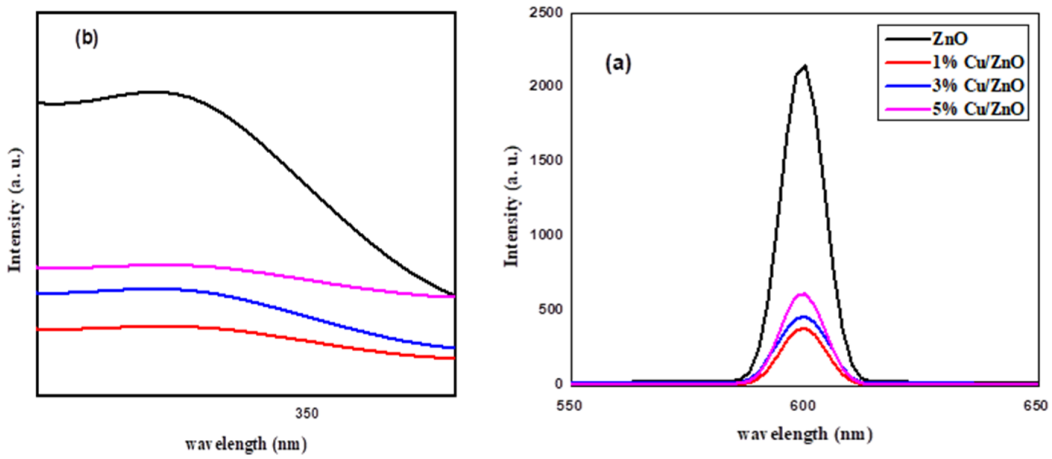

FIG. 5. Photoluminescence spectra of ZnO and Co doped ZnO NPs

3.6. UV-Visible diffuse reflectance spectroscopy studies (DRS UV-Visible) and Tauc plots

The UV-Vis absorption spectra of pure and Cu doped ZnO samples were recorded and presented in Fig. 6(a) The spectra shows increase in absorption ability and red shift with humps as incorporation of Cu content from 1 to 5 mol%. It can be interpreted that there is the formation of new energy levels in the band gap, thereby leading to spectral red shift [23,44]. Therefore the red shift of Cu doped ZnO helps to electron transfer from Zn*3d* to O*2p*. It is observed that the doping effect narrows or shrinks the band gap of ZnO as increasing Cu doping densities.

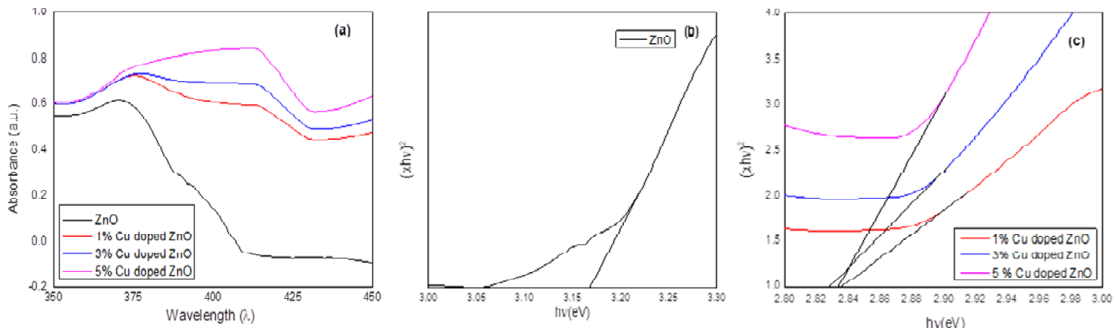

FIG. 6. UV-Visible diffuse reflectance spectrum of ZnO and Cu doped ZnO NPs (a); Tauc plots for band gap determination (b,c)

The Tauc plots Fig. 6(b, c) are drawn using Tauc equation $(\alpha h\nu)^2 = A(h\nu - E_g)$, where, ν is the frequency of light, A is a constant, h is the Planck's constant and E_g is energy band gap of the prepared samples. By extrapolating the line we measure the band gap of prepared ZnO NPs. The computed band gap values are 3.16 for ZnO and 2.84, 2.83, 2.78 eV for 1, 3 and 5 mol% Cu/ZnO respectively i.e. the band gap decreases from 1 to 5 mol%. The absorption edge of samples were associated to the presence of the acceptor level produced by Cu, over the valance band of ZnO [31, 45].

4. Preparationand investigation of dye solution

It is reported that ZnO DSSC are almost unstable in acidic and metal based dyes. Here, we applied sensitization with organic xanthene dyes contain Rose Bengal, Eosin Y. and Rhodamine B. dye. 1:1 proportion of acetonitrile and tert-butanol used to prepare dye solution. UV-Vis absorption investigation Fig. 7 show absorption in visible region at 518, 530, and 535 nm for Eosin Y., Rose Bengal, and Rhodamine-B. Individual dyes have limited absorption so we used mixed dye concept that gives better absorption in the range of 500 – 600 nm which is confirmed by its absorption study [46]. So such sensitization solution is prepared by equal mixing of dyes and sensitization of photoanodes are done.

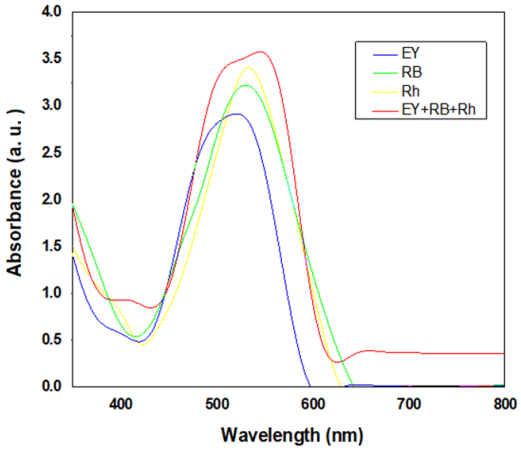

FIG. 7. Optical absorbtion spectra study of single Eosine Y., Rose Bangal, Rhodamine B. dyes and mixed dye in tert-butyl alcohol/acetonitrile

5. Fabrication of photoelectrochemical cell and I–V measurements

5.1. Construction of photoelectrode

Photoelectrodes are prepared by simple doctor blade method [47]. Here NPs were sonicated in alcohol and ethyl cellulose for 30 min. Later α terpineol was added (Sigma-Aldrich) to obtain a better suspension. This suspension deposited on FTO glass surface at conducting side and annealed it at 350 K for 2 h.

5.2. Construction of cell and I–V measurement

The prepared photoanodes are sensitized in dye solution for 12 h and washed with alcohol to remove excess dye. The photoanode of average area 1.0 cm^2 act as working electrode and Pt-coated FTO of similar area were used as the counter electrodes. I–V measurements are taken under under solar simulator standard AM 1.5 one sun illumination visible illumination of 100 mW/cm^2 using a Keithley source meter (model 2460).

First ZnO photoanode without sensitization directly employed in electrolyte solution of 0.1 M lithium iodide and 0.05 M iodine in propylene carbonate then results recorded in dark as well as in light. Later sensitization of ZnO and Cu doped ZnO samples for 12 h carried out and alter I–V measurements are taken Fig. 8. All outcomes i.e. open circuit voltage (V_{oc}), short circuit current density (I_{sc}) and fill factor (FF), efficiency in percentage (η %) are recorded in tabular form in Table 3. It displays worthy efficiency after sensitization i.e. the highest efficiency obtained for 1 % Cu/ZnO of $\eta = 0.1156$ % and other with notable efficiencies 0.0438 and 0.0471 % for 3, 5 % Cu/ZnO respectively.

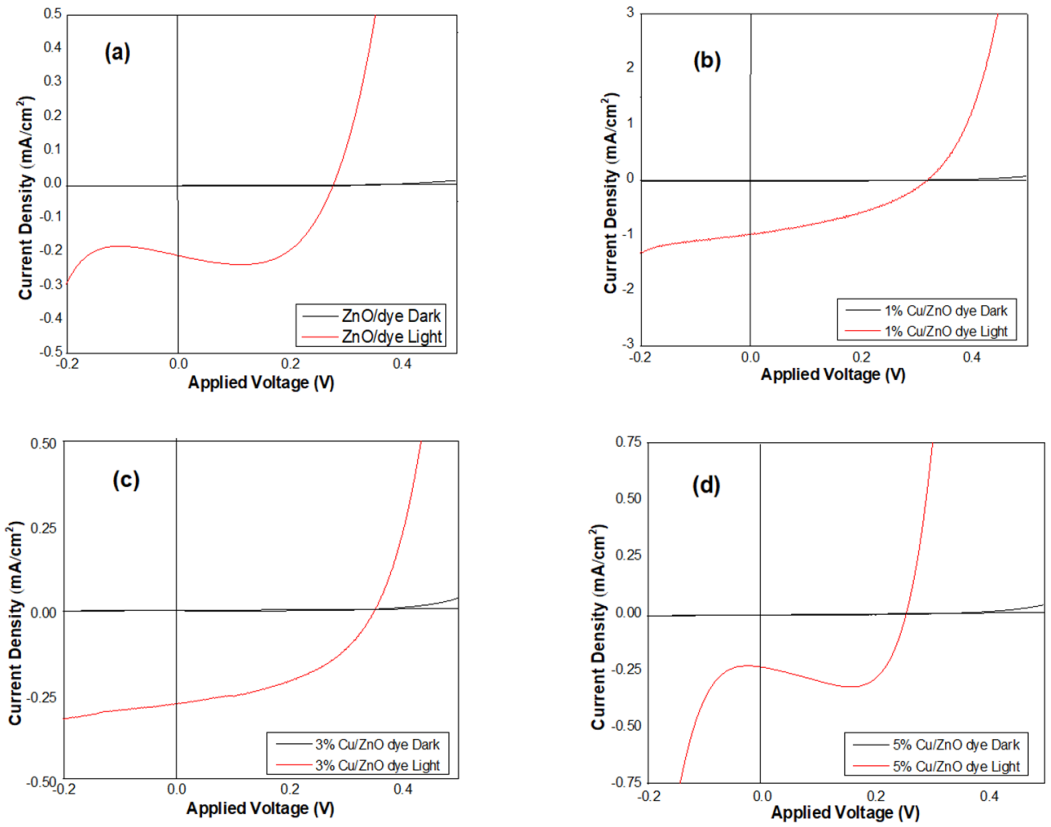

FIG. 8. Photocurrent-voltage curves in I^-/I^{3-} redox electrolyte solution under dark and visible light for: (a) ZnO/dye; (b) 1% Cu/ZnO; (c) 3% Cu/ZnO; (d) 5%Cu/ ZnO with dye

TABLE 3. Photoelectrochemical parameters of the cell

Sample	J_{sc} **(mA/cm^2)**	Voc **(V)**	**FF**	η **%**
ZnO without dye	0.065	0.262	0.27	0.0045
ZnO/dye	0.211	0.278	0.62	0.0363
1 % Cu/ZnO	0.98	0.319	0.37	0.1156
3 % Cu/ZnO	0.277	0.352	0.45	0.0438
5 % Cu/ZnO	0.236	0.256	0.78	0.0471

6. Conclusion

We effectively employed the effective sol gel technique for the synthesis of Cu/ZnO NPs. The XRD and Raman analysis clearly indicated that Cu/ZnO samples possess a hexagonal wurtzite crystal structure. It also revealed the slight decrement of particles and lattice parameters as Cu doping increses in low concentration. Here, nanograin morphologies are formed with respective elemental compositions. FT-IR studies substantiate the presence of the ZnO peaks into the samples with upward shifting due to Cu doping. Photoluminescence (PL) analysis of all samples of ZnO displays peaks at ∼300 nm in the UV range i.e. band edge emission (NBE), and at ∼600 nm in the visible region i.e. deep level emission (DLE). The UV-Vis absorption spectra depicts an increase in absorption ability and red shift with humps as incorporation of Cu content from 1 to 5 mol% while Tauc equation $(\alpha h\nu)^2 = A(h\nu - E_g)$, computed band gap values indicating band gap decrease from 1 to 5 mol% doping i.e 3.16 for ZnO and 2.84, 2.83, 2.78 eV for 1, 3 and 5 mol% Cu/ZnO respectively. I–V measurements of PEC cell is studied that gives notable results with

highest efficiency of $\eta = 0.1156$ % for 1 % Cu/ZnO photoanode with $J_{sc} = 0.98$ mA/cm^2 and $V_{oc} = 0.319$ V. ZnO photoanode without dye sensitization show low η % value, but when it is sensitized, high increment seen for ZnO and 1 % Cu/ZnO but later for 3 and 5 % values found to be decreased. It is may be due intense color of films for high doping that may affect absorption of photon even after sensitization. Photoluminescence studies also indicate higher electron hole recombination for higher doping These outcomes still very low but doping and co-sensitization such working strategy may give another way to enhance DSSCs outcome in the fast growing solar energy sector.

Acknowledgements

This research was made possible by support given by DST-FIST Analytical Instrumentation Laboratory of Lal Bahadur Shastri College, Satara and Jaysingpur College, Jaysingpur, Maharashtra, India.

References

[1] Halsnæs K., Garg A. Assessing the role of energy in development and climate policiesconceptual approach and key indicators. *World Development*, 2011, **39**, P. 987–1001.
[2] Gielen D., Boshell F., et al. The role of renewable energy in the global energy transformation. *Energy Strategy Reviews*, 2019, **24**, P. 38–50.
[3] Panwar N., Kaushik S., Kothari S. Role of renewable energy sources in environmental protection: A review. *Renewable and Sustainable Energy Reviews*, 2011, **15**, P. 1513–1524.
[4] Verbruggen A., Fischedick M., et al. Renewable energy costs, potentials, barriers: Conceptual issues. *Energy policy*, 2010, **38**, P. 850–861.
[5] Ellabban O., Abu-Rub H., Blaabjerg F. Renewable energy resources: Current status, future prospects and their enabling technology. *Renewable and Sustainable Energy Reviews*, 2014, **39**, P. 748–764.
[6] Kabir E., Kumar P., et al. Solar energy: Potential and future prospects. *Renewable and Sustainable Energy Reviews*, 2018, **82**, P. 894–900.
[7] Kannan N., Vakeesan D. Solar energy for future world:–A review. *Renewable and Sustainable Energy Reviews*, 2016, **62**, P. 1092–1105.
[8] Hamann T.W., Jensen R.A., et al. Advancing beyond current generation dye-sensitized solar cells. *Energy & Environmental Science*, 2008, **1**, P. 66–78.
[9] Ye M., Wen X., et al. Recent advances in dye-sensitized solar cells: from photoanodes, sensitizers and electrolytes to counter electrodes. *Mater Today*, 2015, **18**, P. 155–162.
[10] Susanti D., Nafi M., et al. The preparation of dye sensitized solar cell (DSSC) from TiO_2 and tamarillo extract. *Procedia Chemistry*, 2014, **9**, P. 3–10.
[11] Selvaraj P., Baig H., et al. Enhancing the efficiency of transparent dye-sensitized solar cells using concentrated light. *Sol Energy Mater Sol Cells*, 2018, **175**, P. 29–34.
[12] Kumara K.S., Nagaswarupa H., et al. Synthesis and characterization of nano ZnO and MgO powder by low temperature solution combustion method: studies concerning electrochemical and photocatalytic behavior. *Nanosystems: Physics, Chemistry, Mathematics*, 2016, **7**, P. 662–666.
[13] Karuppannan R., Kulandaivel J., Kandasamy J. Zinc oxide-palladium material an efficient solar-light driven photocatalyst for degradation of congo red. *Nanosystems: Physics, Chemistry, Mathematics*, 2016, **7**, P.740–746
[14] Sengupta D., Das P., Mondal B., Mukherjee K. Effects of doping, morphology and film-thickness of photo-anode materials for dye sensitized solar cell application–A review. *Renewable and Sustainable Energy Reviews*, 2016, **60**, P. 356–376.
[15] Bharat T., Mondal S., et al. Synthesis of Doped Zinc Oxide Nanoparticles: A Review. *Materials Today: Proceedings*, 2019, **11**, P. 767–775.
[16] Daksh D., Agrawal Y.K. Rare earth-doped zinc oxide nanostructures: a review. *Reviews in Nanoscience and Nanotechnology*, 2016, **5**, P. 1–27.
[17] Ugwu E.I. The Effect of Annealing, Doping on the Properties and Functionality of Zinc Oxide Thin Film; Review. In: *Sol-Gel Method-Design and Synthesis of New Materials with Interesting Physical Chemical and Biological Properties*, *Intech. Open*, 2018.
[18] Tang K., Gu S.-L., et al. Recent progress of the native defects and p-type doping of zinc oxide. *Chinese Physics B*, 2017, **26**, P. 047702.
[19] Zhang Q., Dandeneau C.S., Zhou X., Cao G. ZnO nanostructures for dye-sensitized solar cells. *Adv. Mater.*, 2009, **21**, P. 4087–4108.
[20] Vittal R., Ho K.-C. Zinc oxide based dye-sensitized solar cells: A review. *Renewable and Sustainable energy reviews*, 2017, **70**, P. 920–935.
[21] Larina L., Alexeeva O.,et al. Very widebandgap nanostructured metal oxide materials for perovskite solar cells. *Nanosystems: Physics, Chemistry, Mathematics*, 2019, **10**, P. 70–75.
[22] Abass N.K.S., Zainab J.S., Mohammed T.H., Abbas L.K. Fabricated of Cu doped ZnO nanoparticles for solar cell application. *Baghdad Science Journal*, 2018, **15**, P. 198–204.
[23] Horzum S., Torun E., Serin T., Peeters F. Structural, electronic and optical properties of Cu-doped ZnO: experimental and theoretical investigation. *Philosophical Magazine*, 2016, **96**, P. 1743–1756.
[24] Joshi K., Rawat M., et al. Band gap widening and narrowing in Cu-doped ZnO thin films. *J. Alloys Compd.*, 2016, **680**, P. 252–258.
[25] Kumari L., Madhuri R., Sharma P.K. Study of structural, optical and electrical properties of hydrothermally synthesised Cu-doped ZnO nanorods. *AIP Conference Proceedings*, AIP Publishing, 2017, P. 050075.
[26] Thankalekshmi R.D.R., Samwad D., Rastogi A.C. Doping sensitive optical scattering in zinc oxide nanostructured films for solar cells. *Advanced Materials Letters*, 2013, **4**, P. 9–14.
[27] Sajjad M., Ullah I., et al. Structural and optical properties of pure and copper doped zinc oxide nanoparticles. *Results in Physics*, 2018, **9**, P. 1301–1309.
[28] Boukaous C., Benhaoua B., Telia A., Ghanem S.J.M.R.E. Effect of copper doping sol-gel ZnO thin films: physical properties and sensitivity to ethanol vapor. *Materials Research Express*, 2017, **4**, 105024.
[29] Rahmati A., Sirgani A.B., Molaei M., Karimipour M.J.T.E.P.J.P. Cu-doped ZnO nanoparticles synthesized by simple co-precipitation route. *The European Physical Journal Plus*, 2014, **129**, P. 250.
[30] Sharma P.K., Dutta R.K., Pandey A.C. Doping dependent room-temperature ferromagnetism and structural properties of dilute magnetic semiconductor ZnO: Cu2+ nanorods. *Journal of Magnetism and Magnetic Materials*, 2009, **321**, P. 4001–4005.

[31] Tyona M., Osuji R., et al. Highly efficient natural dye-sensitized photoelectrochemical solar cells based on Cu-doped zinc oxide thin film electrodes. *Adv. Appl. Sci. Res.*, 2015, **6**, P. 7–20.

[32] Daratika D.A., Baqiya M.A. Synthesis of $Zn_{1-x}Cu_xO$ Nanoparticles by Coprecipitation and Their Structure and Electrical Property. *IOP Conference Series: Materials Science and Engineering*, IOP Publishing, 2017, P. 012009.

[33] Das B.K., Das T., et al. Structural, bandgap tuning and electrical properties of Cu doped ZnO nanoparticles synthesized by mechanical alloying. *Journal of Materials Science: Materials in Electronics*, 2017, **28**, P. 15127–15134.

[34] Pung S., Ong C., Isha K.M., Othman M.J.S.M. Synthesis and characterization of Cu-doped ZnO nanorods. *Sains Malaysiana*, 2014, **43**, P. 273–281.

[35] Djouadi D., Slimi O., et al. Effects of (Ce, Cu) Co-doping on the Structural and Optical Properties of ZnO Aerogels Synthesized in Supercritical Ethanol. *Journal of Physics: Conference Series*, IOP Publishing, 2018, P. 012008.

[36] Vaiano V., Iervolino G., Rizzo L.J.A.C.B.E. Cu-doped ZnO as efficient photocatalyst for the oxidation of arsenite to arsenate under visible light. *Applied Catalysis B: Environmental*, 2018, **238**, P. 471–479.

[37] Chow L., Lupan O., et al. Synthesis and characterization of Cu-doped ZnO one-dimensional structures for miniaturized sensor applications with faster response. *Sensors and Actuators A: Physical*, 2013, **189**, P. 399–408.

[38] Joshi K., Rawat M., et al. Band gap widening and narrowing in Cu-doped ZnO thin films. *Journal of Alloys and Compounds*, 2016, **680**, P. 252–258.

[39] Abinaya C., Marikkannan M., et al. Structural and optical characterization and efficacy of hydrothermal synthesized Cu and Ag doped zinc oxide nanoplate bactericides. *Materials Chemistry and Physics*, 2016, **184**, P. 172–182.

[40] Muthukumaran S., Gopalakrishnan R. Structural, FTIR and photoluminescence studies of Cu doped ZnO nanopowders by co-precipitation method. *Opt. Mater.*, 2012, **34**, P. 1946–1953.

[41] Moussawi R.N., Patra D. Modification of nanostructured ZnO surfaces with curcumin: fluorescence-based sensing for arsenic and improving arsenic removal by ZnO. *RSC Advances*, 2016, **6**, P. 17256–17268.

[42] Chow L., Lupan O., et al. Synthesis and characterization of Cu-doped ZnO one-dimensional structures for miniaturized sensor applications with faster response. *Sensors and Actuators A: Physical*, 2013, **189**, P. 399–408.

[43] Kuriakose S., Satpati B., Mohapatra S. Highly efficient photocatalytic degradation of organic dyes by Cu doped ZnO nanostructures. *Phys. Chem. Chem. Phys.*, 2015, **17**, P. 25172–25181.

[44] Kadam A., Kim T.G., et al. Morphological evolution of Cu doped ZnO for enhancement of photocatalytic activity. *J. Alloys Compd.*, 2017, **710**, P. 102–113.

[45] Bandyopadhyay P., Dey A., et al. Synthesis and characterization of copper doped zinc oxide nanoparticles and its application in energy conversion. *Current Applied Physics*, 2014, **14**, P. 1149–1155.

[46] Sharma K., Sharma V., Sharma S. Dye-sensitized solar cells: fundamentals and current status. *Nanoscale research letters*, 2018, **13**, P. 381.

[47] Wood C.J., Summers G.H., et al. A comprehensive comparison of dye-sensitized NiO photocathodes for solar energy conversion. *Phys. Chem. Chem. Phys.*, 2016, **18**, P. 10727–10738.